levels in C26 cells compared with normal cells. Therefore, NO-HSA may show selective cytotoxicity for tumor cells and not affect normal cells. These findings strongly suggest that NO-HSA is a promising therapeutic anticancer agent, given the unusual redox conditions typical of malignant cells.

Antiapoptotic effects of NO have been observed in a variety of cells, including T cells, hepatocytes, endothelial cells, neurons, ovarian follicle cells, eosinophils, thymocytes, and embryonic kidney cells (Liu and Stamler, 1999). In a recent study using U937 human promonocytic cells, NO-R410C (a genetic variant of HSA) had antiapoptotic activity (Ishima et al., 2007). Whether NO ultimately inhibits or promotes apoptosis probably depends on the cell, the signal, the source, the molecule, the amount, and the presence or absence of coreactants. For example, the amount of NO bound to the carrier molecule seems to account for the discrepant results between previous investigations and the present study. The NO content of NO-R410C (in the previous study) and NO-HSA (in this study) were 1.3 and 6.6 mol NO/mol HSA, respectively, and the *S*-nitroso moiety concentrations in vitro were 26 to 130 and 165 to 660 μM, respectively. Mohr et al. (1997) reported that 10 to 100 μM GSNO inhibits the activation of caspase-3 induced by actinomycin D in U937 cells. In contrast, apoptosis (characterized by DNA fragmentation and morphological changes) was observed in U937 cells treated with GSNO at concentrations in excess of 250 μM (Messmer et al., 1996). Based on the results of the present study and those of previously published investigations, the critical NO threshold concentration between promotion and inhibition of apoptosis seems to be 100 to 200 μM.

Matsumura et al. (1987) examined the accumulation of differently sized proteins within tumor tissues of tumor-bearing mice. Macromolecules containing HSA tended to accumulate in tumor tissues, apparently due to hypervascularization and enhanced vascular permeability (even to macromolecules) of the tumors, with little export of macromolecules from the tumor tissue via blood or lymphatic vessels (Matsumura et al., 1987). Therefore, NO-HSA may be a useful agent for targeting chemotherapeutics to tumor tissue. However, the short half-life of NO has been one of the greatest obstacles to therapeutic application of NO donors. Consequently, the pharmacokinetic properties of NO-HSA in mice were measured to determine the biological fate of NO. The apparent half-life of *S*-nitroso moieties in NO-HSA was estimated to be 18.9 min (data not shown), which is similar to that of NO-R410C, but much longer than that of the low-molecular-weight NO donor GSNO (4.2 min) (Ishima et al., 2007). In the present study, the difference in NO half-life between NO-HSA and GSNO seemed to be due to reduced renal excretion of HSA compared with glutathione due to its larger molecular size, suggesting that HSA may be a useful NO carrier in vivo.

In summary, NO-HSA was synthesized by inducing *S*-nitrosothiol linkages using iminothiolane as a spacer. NO-HSA generated ROS in C26 cells, and it induced intrinsic apoptotic events, such as depolarization of mitochondrial membrane potentials, activation of caspase-3, and induction of DNA fragmentation. Moreover, NO-HSA inhibited proliferation of tumor cells in vitro in a concentration-dependent manner. In the in vivo experiments, NO-HSA also strongly inhibited tumor growth by inducing apoptosis, with no side effects. The results of the present study suggest that NO-HSA has promise as a new generation anticancer agent with few side effects.

References

Azuma H, Ishikawa M, and Sekizaki S (1986) Endothelium-dependent inhibition of platelet aggregation. *Br J Pharmacol* **88**:411–415.

Beckman JS and Crow JP (1993) Pathological implication of nitric oxide, superoxide and peroxnitrite formation. *Biochem Soc Trans* **21**:330–334.

Brune B, Sandau K, and Knethen AV (1998) Apoptotic cell death and nitric oxide: activating and antagonistic transducing pathways. *Biochemistry (Mosc)* **63**:817–825.

Chen RF (1967) Removal of fatty acids from serum albumin by charcoal Treatment. *J Biol Chem* **242**:173–181.

Ewing JF, Young DV, Janero DR, Garvey DS, and Grinnell TA (1997) Nitrosylated bovine serum albumin derivatives as pharmacologically active nitric oxide congeners. *J Pharmacol Exp Ther* **283**:947–954.

Fabbri F, Brigliadori G, Ulivi P, Tesei A, Vannini I, Rosetti M, Bravaccini S, Amadori D, Bolla M, and Zoli W (2005) Pro-apoptotic effect of a nitric oxide-donating NSAID, NCX4040, on bladder carcinoma cells. *Apoptosis* **10**:1095–1103.

Feng R, Ni HM, Wang SY, Tourkova IL, Shulin MR, Harada H, and Yin XM (2007) Cyanidin-3-rutinoside, a natural polyphenol antioxidant, selectively kills leukemic cells by induction of oxidative stress. *J Biol Chem* **282**:13468–13476.

Gao J, Liu X, and Rigas B (2005) Nitric oxide-donating aspirin induces apoptosis in human colon cancer cells through induction of oxidative stress. *Proc Natl Acad Sci U S A* **102**:17207–17212.

Garthwaite J (1991) Glutamate, nitric oxide and cell-cell signaling in the nervous system. *Trends Neurosci* **14**:60–67.

Gavrieli Y, Sherman Y, and Ben-Sasson SA (1992) Identification of programmed cell death in Situ via specific labeling of nuclear DNA fragmentation. *J Cell Biol* **119**:493–501.

Hibbs JB Jr, Taintor RR, Vavrin Z, and Rachlin EM (1988) Nitric oxide: a cytotoxic activated macrophage effector molecule. *Biochem Biophys Res Commun* **157**:87–94.

Ignarro LJ (1989) Endothelium-derived nitric oxide–pharmacology and relationship to the actions of organic nitrate esters. *Pharm Res* **6**:651–659.

Ishima Y, Sawa T, Kragh-Hansen U, Miyamoto Y, Matsushita S, Akaike T, and Otagiri M (2007) *S*-Nitrosylation of human variant albumin Liprizzi (R410C) confers potent antibacterial and cytoprotective properties. *J Pharmacol Exp Ther* **320**:969–977.

Ishiyama M, Tominaga H, Shiga M, Sasamoto K, Ohkura Y, and Ueno K (1996) A combined assay of cell viability and in vitro cytotoxicity with a highly water-soluble tetrazolium salt, neutral red and crystal violet. *Biol Pharm Bull* **19**:1518–1520.

Kashfi K, Ryann Y, Qiao LL, Williams JL, Chen J, Soldato PD, Traganos FT, and Rigas B (2002) Nitric oxide-donating nonsteroidal anti-inflammatory drugs inhibit the growth of various cultured human cancer cells: evidence of a tissue type-independent effect. *J Pharmacol Exp Ther* **303**:1273–1282.

Kaufmann SH and Gores GJ (2000) Apoptosis in cancer: cause and cure. *Bioessays* **22**:1007–1017.

Kiziltepe T, Hideshima T, Ishitsuka K, Ocio EM, Raje N, Catley L, Li CQ, Trudel LJ, Yasi H, Vallet S, et al. (2007) JS-K, a GST-activated nitric oxide generator, induces DNA double-strand breaks, activates DNA damage response pathways, and induces apoptosis in vitro and in vivo in human multiple myeloma cells. *Blood* **110**:709–718.

Kondo Y, Kanzawa T, Sawaya R, and Kondo S (2005) The role of autophagy in cancer development and response to therapy. *Nat Rev Cancer* **5**:726–734.

Laval F and Wink DA (1994) Inhibition by nitric oxide of the repair protein, O6-methyl-gluanine-DNA-methyltransferase. *Carcinogenesis* **15**:443–447.

Liu L and Stamler JS (1999) NO: an inhibitor of cell death. *Cell Death Differ* **6**:937–942.

Marks DS, Vita JA, Folts JD, Keaney JF Jr, Welch GN, and Loscalzo J (1995). Inhibition of neointimal proliferation intimal proliferation in rabbits after vascular injury by a single treatment with a protein adduct of nitric oxide. *J Clin Investig* **96**:2630–2638.

Marletta MA, Yoon PS, Iyengar R, Leaf CD, and Wishnok JS (1988) Macrophage oxidation of L-arginine to nitrite and nitrate–nitric oxide is an intermediate. *Biochemistry* **27**:8706–8711.

Matsumura Y, Oda T, and Maeda H (1987) General mechanism of intratumor accumulation of macromolecules: advantage of macromolecular therapeutics. *Gan To Kagaku Ryoho* **14**:821–829.

Matsushita S, Ishima Y, Chuang VT, Watanabe H, Tanase S, Maruyama T, and Otagiri M (2004) Functional analysis of recombinant human serum albumin domains for pharmaceutical applications. *Pharm Res* **10**:1924–1932.

Messmer UK, Reimer DM, and Brune B (1996) Nitric oxide-induced apoptosis: p53-dependent and p53-indeoendent signaling pathways. *Biochem J* **319**:299–305.

Meng XW, Lee SH, and Kaufmann SH (2006) Apoptosis in the treatment of cancer: a promise kept? *Curr Opin Cell Biol* **18**:668–676.

Mohr S, Zech B, Lapetina EG, and Brune B (1997) Inhibition of caspase-3 by S-nitrosation and oxidation caused by Nitric oxide. *Biochem Biophys Res Commun* **238**:387–391.

Moncada S and Higgs A (1993) The L-arginine-nitric oxide pathway. *N Engl J Med* **329**:2002–2012.

Moncada S, Palmar RMJ, and Gryglewski RJ (1986) Mechanism of action of some inhibitors of endothelium-derived relaxing factor. *Proc Natl Acad Sci U S A* **83**:9164–9168.

Okada H and Mak TW (2004) Pathways of apoptotic and non-apoptotic death in tumor cells. *Nat Rev Cancer* **4**:592–603.

Peters T Jr (1985) Serum albumin. *Adv Protein Chem* **37**:161–245.

Ramachandran N, Root P, Jiang XM, Hogg OJ, and Mutus B (2001) Mechanism of

transfer of NO from extracellular S nitrosothiols into the cytosol by cell-surface protein disulfide isomerase. *Proc Natl Acad Sci U S A* **98**:9539–9544.

Schumacker PT (2006) Reactive oxygen species in cancer cells: live by sword, die by the sword. *Cancer Cell* **10**:175–176.

Semsroth S, Fellner B, Trescher K, Bernecker OY, Kalinowski L, Gasser H, Hallstrom S, Malinski T, and Podesser BK (2005) S-Nitroso human serum albumin attenuates ischemia/reperfusion injury after cardioplegic arrest in isolated rabbit hearts. *J Heart Lung Transplant* **24**:2226–2234.

Shimizu K, Asai T, Fuse C, Sadzuka Y, Sonobe T, Ogino K, Taki T, Tanaka T, and Oku N (2005) Applicability of anti-neovascular therapy to drug-resistant tumor: suppression of drug-resistant P388 tumor growth with neovessel-targeted liposomal adriamycin. *Int J Pharm* **296**:133–141.

Simon DI, Mullins ME, Jia L, Gaston B, Singel DJ, and Stamler JS (1996) Polynitrosylated proteins: characterization, bioactivity, and functional consequences. *Proc Natl Acad Sci U S A* **93**:4736–4741.

Stamler JS, Jaraki O, Osborne J, Simon DI, Keaney J, Vita J, Singel D, Valeri CR, and Loscalzo J (1992) Nitric oxide circulates in mammalian plasma primarily as an S-nitroso adduct of serum albumin. *Proc Natl Acad Sci U S A* **89**:7674–7677.

Trachootham D, Zhou Y, Zhang H, Demizu Y, Chen Z, Pelicano H, Chiao PJ, Achanta G, Arlinghaus RB, Liu J, et al. (2006) Selective killing of oncogenically transformed cells through a ROS-mediated mechanism by β-phenylethyl isothiocyanate. *Cancer Cell* **10**:241–252.

Williams JL, Borgo S, Hasan I, CastilloE, Traganos F, and Rigas B (2001) Nitric oxide-releasing nonsteroidal anti-inflammatory drugs (NSAIDs) alter the kinetics of human colon cancer cell lines more effectively than traditional NSAIDs: implication for colon cancer chemoprevention. *Cancer Res* **61**:3285–3289.

Wong PS and Fukuto JM (1999) Reaction of organic nitrate esters and S-nitrosothiols with reduced flavins: a possible mechanism of bioactivation. *Drug Metab Dispos* **27**:502–509.

Address correspondence to: Dr. Masaki Otagiri, Department of Biopharmaceutics, Graduate school of Pharmaceutical Sciences, Kumamoto University, 5-1 Oe-honmachi, Kumamoto 862-0973, Japan. E-mail: otagirim@gpo.kumamoto-u.ac.jp

日本胸部臨床 麻酔 形成外科 の書籍案内・ご購入と書籍検索

克誠堂出版

〒113-0033 東京都文京区本郷3-23-5-202
TEL.03-3811-0995 / FAX.03-3813-1866

周術期輸血

高折　益彦　著

B5判・250頁
定価7,350円（本体7,000円＋税5%）2007年
ISBN978-4-7719-0321-0
【書籍名】周術期輸血
【品番コード】00321

・血液製剤の投与によっていかに組織酸素代謝を維持するか。

・いかに止血を的確に行うか。

周術期で必要な輸血学、輸血医療の基本を身につけたいなら。

目次

III. 血液型

IV. 輸血療法の実際

V. 輸血事故，輸血副作用・合併症

VI. 自己血輸血

VII. 人工血液

VIII. 輸血医療に関連した法的規則事項

IX. 輸血に関連する歴史的事項

その他のシリーズはこちら->

このページのtopに戻る

| ホーム | 書籍購入の方法 | 会社案内 | 本郷昔語り | サイトマップ | お問い合わせ |

Available online at www.sciencedirect.com
ScienceDirect
Biomaterials 28 (2007) 2655–2666
Biomaterials
www.elsevier.com/locate/biomaterials

Selective uptake of surface-modified phospholipid vesicles by bone marrow macrophages *in vivo*

Keitaro Sou[a], Beth Goins[b], Shinji Takeoka[a], Eishun Tsuchida[a,*], William T. Phillips[b]

[a]*Advanced Research Institute for Science and Engineering, Waseda University, Tokyo 169-8555, Japan*
[b]*Department of Radiology, University of Texas Health Science Center at San Antonio, 7703 Floyd Curl Drive, San Antonio, TX 78229-3900, USA*

Received 29 August 2006; accepted 31 January 2007
Available online 20 February 2007

Abstract

An advantage of using vesicles (liposomes) as drug delivery carriers is that their pharmacokinetics can be controlled by surface characteristics, which can permit specific delivery of the encapsulated agents to organs or cells *in vivo*. Here we report a vesicle formulation which targets the bone marrow after intravenous injection in rabbits. Surface modification of the vesicle with an anionic amphiphile; L-glutamic acid, *N*-(3-carboxy-1-oxopropyl)-, 1,5-dihexadecyl ester (SA) results in significant targeting of vesicles to bone marrow. Further incorporation of as little as 0.6 mol% of poly(ethylene glycol)-lipid (PEG-DSPE) passively enhanced the distribution of SA-vesicles into bone marrow and inhibited hepatic uptake. In this model, more than 60% of the intravenously injected vesicles were distributed to bone marrow within 6 h after administration of a small dose of lipid (15 mg/kg b.w.). Histological evidence indicates that the targeting was achieved due to uptake by bone marrow macrophages (BMMϕ). The efficient delivery of encapsulated scintigraphic and fluorescent imaging agents to BMMϕ suggests that vesicles are promising carriers for the specific targeting of BMMϕ and may be useful for delivering a wide range of therapeutic agents to bone marrow.

Keywords: Nanoparticle; Liposome; Bone marrow; Macrophage; Drug delivery; Surface modification

1. Introduction

Nanoparticulate carrier systems have been investigated as candidates for targeted delivery in cancer therapy and gene therapy [1,2]. A wide variety of nanoparticle systems have been developed for biological applications. One of the advantages of using nanoparticulate materials is based on their controllable surface properties which permit specific interactions with cells, tissues, and organs. Although a number of investigators have demonstrated that endocytosis of nanoparticles *in vitro* is accelerated by surface modification of the particles with specific ligands, the specific *in vivo* targeting of cells remains challenging because it is hindered by competing interactions, especially fairly high mononuclear phagocyte system (MPS) uptake *in vivo*.

Phospholipid vesicles (liposomes) have been widely investigated as potential carriers for drugs, genes, and proteins because their capsular structure permits encapsulation of various therapeutic agents [2–4]. Because of their particulate nature, these vesicles are trapped in the MPS, particularly hepatic Kupffer cells and spleen macrophages following intravenous administration [5,6]. Once in the bloodstream, the binding of plasma proteins such as immunoglobulins, complement proteins, apolipoproteins, etc., which together are termed "opsonins" on the vesicular surface have been reported to accelerate phagocytosis of the vesicles by macrophages, because the macrophages have scavenger receptors to bind the opsonins [5]. In addition to this mechanism, vesicles containing anionic phospholipids such as phosphatidylserine (PS), which are markers of apoptotic cells, have been reported to bind with a PS receptor on macrophages [7]. Improved vesicles with

*Corresponding author. Tel.: +81 3 5286 3120; fax: +81 3 3205 4740.
E-mail addresses: ksou@waseda.jp (K. Sou), eishun@waseda.jp (E. Tsuchida).

0142-9612/$ - see front matter © 2007 Elsevier Ltd. All rights reserved.
doi:10.1016/j.biomaterials.2007.01.041

prolonged circulation times preventing MPS uptake have been formulated with poly(ethylene glycol) (PEG) derivatives [8]. These vesicles have been termed as stealth liposomes, due to their ability to evade uptake by the macrophage, particularly Kupffer cells. Long circulating liposomes with PEG surface modification are currently being used as anti-cancer drug delivery agents [9].

On the other hand, the phagocytic ability of the MPS contributes to achieving an active targeting of particulate carriers to macrophages [10,11]. Macrophages produce a wide range of biologically active molecules that are both beneficial and detrimental. Many of the detrimental effects of macrophages are associated with their pro-inflammatory effects. Thus, interventions targeted to macrophages may open new therapeutic approaches for controlling diseases associated with inflammation. Evidence from a number of sources suggests that cancer-associated inflammation promotes tumor growth and progression, and tumor-associated macrophages play a critical role in the initiation, maintenance, and resolution of inflammation [12]. These tumor-associated macrophages are inactivated by mediators from tumor cells, and they serve to promote tumor growth. The importance of macrophages in disease development has led a number of researchers to investigate methods for the site-specific delivery of drugs to macrophages.

Bone marrow, which contains macrophages, is one of the organs responsible for uptake of circulating particulate materials [5,9,13–17]. Also, macrophages associated with erythroblasts in a hematopoietic environment participate in erythropoiesis control, and engulfment of nuclei from erythroid precursor cells [18,19]. The development of drug delivery systems with specific bone marrow targeting may have therapeutic benefits for hematological malignancies as well as hemopoiesis control. However, very little attention has been paid to bone marrow as part of the MPS because its contribution to the overall MPS is generally much less than that of the liver and spleen *in vivo*. Another essential problem for targeting of BMMϕ is caused by lack of understanding of their specific targeting receptor. Therefore, development of a method for specifically targeting bone marrow will be facilitated by knowledge of the strategies to allow nanoparticles to escape from liver and spleen uptake, but not from bone marrow uptake, and development of specific ligands to induce targeting of bone marrow MPS.

Recently, we have discovered a vesicular formulation which shows remarkable targeting to rabbit bone marrow even when administered at small lipid doses. In this article, we address the components of this vesicle responsible for the targeting of bone marrow and additional vesicular modifications for escaping from liver and spleen uptake, but not from bone marrow. These results may be widely applied to the design of nanoparticulate carriers that target the bone marrow. Bone marrow targeting carriers could open up a wide variety of new therapeutic applications.

2. Materials and methods

2.1. Materials

1,2-Dipalmitoyl-*sn*-glycero-3-phosphocholine (DPPC) and cholesterol (CH) were purchased from Nippon Fine Chemical Co. Ltd. (Osaka, Japan); 1,2-distearoyl-*sn*-glycero-3-phosphoethanolamine-*N*-[monomethoxy poly(ethylene glycol) (5000)] (PEG-DSPE) was purchased from NOF Co. (Tokyo, Japan). L-glutamic acid, *N*-(3-carboxy-1-oxopropyl)-, 1,5-dihexadecyl ester (SA) was synthesized as previously reported [20]. Glutathione was purchased from Sigma (St. Louis, MO). Superoxide dismutase (SOD) was purchased from Wako Pure Chemical Industries Ltd. (Osaka, Japan). 4,4-difluoro-5-methyl-4-bora-3a,4a-diaza-s-indacene-3-dodecanoic acid (C_1-BODIPY C_{12}) and Texas Red (TR) sulfonyl chloride were purchased from Molecular Probes, Inc. (Eugene, OR).

2.2. Preparation of vesicles

All vesicle preparations were performed under sterile conditions. DPPC and CH (1:1 molar ratio), or DPPC, CH, and SA (1:1:0.2 molar ratio) were dissolved in benzene and lyophilized to lipid powders. The mixed lipid powder was hydrated with a glutathione (30 mM) and NaCl (120 mM) solution (pH: 7.0) at 5 g dL^{-1}, and submitted to three cycles of freeze–thawing. After controlling vesicle size by an extrusion method (final pore size of the filter: 0.22 μm, Fuji microfilter, Fuji Photo Film Co., Tokyo, Japan), the unencapsulated glutathione was removed by three ultracentrifugation steps ($3 \times 10^5 g$, 60 min each) and the vesicles were dispersed in saline solution. Surface modification with PEG was performed by making use of the spontaneous incorporation of PEG-DPSE into vesicles [21]. Various concentrations of the PEG-DSPE dispersion were added to the vesicle dispersion and the mixture incubated at 37 °C for 3 h. The vesicle dispersion was ultracentrifuged ($3 \times 10^5 g$, 60 min) to remove unincorporated PEG-DSPE in the supernatant. After washing the precipitated vesicle pellet by ultracentrifugation ($3 \times 10^5 g$, 60 min), the PEG-modified vesicles (PEG-vesicles) were dispersed in saline at 7 g dL^{-1}, and the dispersion was then passed through a sterilized membrane filter (pore size 0.45 μm, DISMIC filter 45, ADVANTEC). The amount of PEG-DSPE incorporated was determined from the peak area ratio of methylene protons of PEG-DSPE (3.63 ppm) to the choline methyl protons of DPPC (3.39 ppm) using ^{1}H-NMR spectroscopy (JEOL JNM-LA500) [21]. SA-vesicles containing 0.3, 0.6, 1.4, and 2.6 mol% of PEG-DSPE on the surface (represented as PEG(0.3)-, PEG(0.6)-, PEG(1.4)-, and PEG(2.6)-[SA-Ve], respectively) and control vesicles containing 2.6 mol% of PEG-DSPE (represented as PEG(2.6)-Ve) were prepared and characterized for these studies. The diameter of the resulting vesicles was determined with a COULTER submicron particle analyzer (N4SD, Coulter, Hialeah, FL), and represented as an average diameter ± standard deviation (SD). Endotoxin contamination was determined to be below 0.1 EU/mL by the Limulus assay test [22].

2.3. Technetium-99m (^{99m}Tc)-labeling of vesicles

Radiolabeling of vesicles was performed according to a method described previously [14,17,23,24]. A saline solution of sodium [^{99m}Tc]pertechnetate (5 mL, 2.78 GBq (75 mCi)) (GE Healthcare Radiopharmacy, San Antonio, TX) was injected into a vial containing lyophilized hexamethylpropyleneamine oxime (HMPAO; 0.5 mg, $SnCl_2$; 7.6 μg) (Ceretec™; GE Healthcare, Arlington, IL). The mixed solution was incubated for 5 min at room temperature. The ^{99m}Tc-HMPAO solution (1 mL) was then added to the vesicle dispersion ([lipids] = 7 g dL^{-1}, 1 mL), and the resulting mixture was incubated for 1 h. After removing free ^{99m}Tc-HMPAO by gel filtration (Sephadex-G25 column), total radioactivity was measured in a dose calibrator (Radex, Mark 5 Model, Houston, TX) and the labeling efficiency was calculated as the percentage of radioactivity in ^{99m}Tc-vesicles to radioactivity measured just before gel filtration.

2.4. Labeling stability of ^{99m}Tc-labeled vesicles in vitro

Labeling stability was examined *in vitro* according to a previously reported procedure [25]. Prepared ^{99m}Tc-labeled vesicle dispersions (0.5 mL) were mixed with rabbit serum (1.5 mL) and incubated at 37 °C to check the labeling stability. A 100 μL aliquot of incubated sample at 24 and 48 h after mixing was passed through a Bio Gel A-15 m (200–400 mesh) spin column. The sample was eluted by sequential addition of 100 μL of Dulbecco's phosphate-buffered saline (pH 7.3) under the centrifugal force of 1000 rpm for 1 min. Each fraction was collected separately and counted in a scintillation well counter (Canberra multichannel analyzer; Canberra Industries, Meriden, CT). Another 100 μL aliquot of incubation sample was used as a standard. The sum total of activity eluted with vesicle fractions was compared with total radioactivity in the standard. As for ^{99m}Tc-labeled PEG(0.6)-[SA-Ve], the labeling stability was also examined in human plasma at 37 °C for 24 h.

2.5. Animal experiments

Animal experiments were performed under the National Institutes of Health Animal Use and Care guidelines and approved by the University of Texas Health Science Center at San Antonio Institutional Animal Care Committee. Male New Zealand White rabbits (2–3 kg, $n = 3$–4 per each vesicle formulation) were anesthetized with an intramuscular injection of ketamine/xylazine (both from Phoenix Scientific, St. Joseph, MO) mixture (50 and 10 mg/kg body weight (b.w.), respectively). One ear of a rabbit was catheterized with a venous line, and the other ear was catheterized with an arterial line. ^{99m}Tc-vesicles were infused into the venous line at 1 mL/min and blood samples were drawn from the arterial line. Each rabbit received a total dose of 214.6–377.4 MBq (5.8–10.2 mCi) ^{99m}Tc-activity and 15 mg/kg b.w. of lipids. As a control study, ^{99m}Tc-HMPAO solution (3 mL) was mixed with glutathione solution (30 mM, 3 mL), and the mixed solution was infused into the venous line at 1 mL/min in rabbits. Each rabbit received a total dose of 321.9–399.6 MBq (8.7–10.8 mCi) ^{99m}Tc-activity.

2.6. Imaging study

Rabbits were placed in the supine position under a Picker (Cleveland, OH) large-field-of-view gamma camera using a low-energy all-purpose collimator and interfaced with a Pinnacle imaging computer (Medasys, Ann Arbor, MI). One-minute dynamic 64 × 64 pixel scintigraphic images were acquired over a continuous period of 1.5 h after the injection of ^{99m}Tc-vesicles. Static images were also acquired at various times post-injection. The image analysis was performed using a nuclear medicine analysis workstation (Pinnacle computer; Medasys, Ann Arbor, MI). The regions of interest were drawn around images of the whole body, one femur, liver, and spleen. The radioactivity counts were decay-corrected at each time, and converted to a percentage of whole body counts. Corrections were made for the blood pool contribution of each organ using the percent injected dose (%ID) measured immediately after infusion.

2.7. Blood persistence and biodistribution

Blood was collected from the arterial line of the rabbit (100 μL) at various times post-injection. The radioactivity of blood samples was quantified in a scintillation well counter (Canberra Multichannel Analyzer, Meridan, CT) during the same counting session. The counts at each time were converted to the percentage of the counts in the sample collected immediately after injection. The animals were rapidly sacrificed at 6 or 24 h and the tissue samples were collected, weighed and counted for radioactivity in the same scintillation well counter for calculation of biodistribution. To calculate the %ID per organ, total blood volume, muscle and skin mass were estimated as 5.7%, 45%, and 10% of total body weight, respectively [26,27]. Bone mass was estimated to be 12 times that of one femur [28].

2.8. Microscopic study

Histological examination of fluorescence delivered into bone marrow tissues was performed using PEG(0.6)-[SA-Ve], double fluorescently labeled by encapsulating SOD conjugated by TR sulfonyl chloride (TR-SOD) in inner aqueous phase and embedding C_1-BODIPY C_{12} in bilayer membrane. Conjugation of TR-SOD to SOD was performed according to previously reported procedure [29], and purified TR-SOD was encapsulated in mixed lipids including 1 mol% of C_1-BODIPY C_{12} to obtain the double fluorescently-labeled PEG(0.6)-[SA-Ve] with size of 247 ± 22 nm in diameter. Labeled vesicles were i.v. injected into anesthetized Male New Zealand White rabbits (2.5 kg, lipids: 15 mg/kg b.w.). At 6 h after injection, femoral bone marrow tissues, liver and spleen were taken, fixed in 10% formalin solution, and then sliced into sections. The sections were fixed on the glass slides with agar at 4 °C and examined with a confocal scanning microscope (Olympus IX-70). Transmission electron microscopic (TEM) observation was performed to observe the bone marrow tissues at a higher magnification. PEG(0.6)-[SA-Ve] were i.v. injected into anesthetized Male New Zealand White rabbits (2.5 kg). The rabbits received 15 mg/kg b.w. of lipids. Control rabbits received no injection. Bone marrow was taken from the left femur of rabbits at 6 h after injection of vesicles, and fixed in 2.5% glutaraldehyde solution. The fixed bone marrow was then washed with 0.1 mol/L phosphate buffer, pH 7.4, and stained with 2% osmic acid solution at 4 °C for 2 h. The organs were first dehydrated stepwise with ethanol, and then polymerized using Quetol 812 at 60 °C for 28 h. The obtained samples were sliced into sections by using an Ultracut S microtome. The sliced samples were stained with 3% uranyl acetate solution for 20 min and then treated with Satoh's lead solution (lead acetate, lead nitrate, and lead citrate) in citrate for 5 min, washed, and dried. The sample was observed and a picture taken with a transmission electron microscope (TEM, H-7500, Hitachi, Tokyo, Japan).

2.9. Theoretical estimation

The theoretical estimation for surface coverage by PEG on vesicles has been reported previously [30,31]. At low grafting densities of PEG, the chains of grafted-PEG are displayed "mushrooms", in which area A_{PEG} covered by each molecule is theoretically calculated as

$$A_{PEG} = \pi R_F^2, \tag{1}$$

where the Flory radius R_F is given by

$$R_F = N^{3/5} a, \tag{2}$$

where N is the degree of polymerization, a is the size of a monomer.

The percentage of covered surface area by PEG in the mushroom conformation R was estimated as

$$R = A_{PEG} \times M / A_{lipid}, \tag{3}$$

where M is the mole percentage of PEG-DSPE and A_{lipid} is the average area of total membrane lipids. In subsequent calculation, we used $N = 114$ and $a = 0.35$ nm for PEG (Mw 5000), and $A_{lipid} \approx 0.4\,nm^2$ for average area as mixed membrane of DPPC and CH (1:1 molar ratio) [32].

2.10. Statistical methods

Values are reported as mean ± standard error of the mean (SEM). Statistical analysis was performed using Microsoft Excel for Windows. Biodistribution data were compared using the Student's unpaired t-test. A p-value <0.01 or 0.05 was considered statistically significant.

3. Results

3.1. Surface modification and radiolabeling

The average diameter of vesicles was controlled to 270 nm by the stepwise extrusion through cellulose acetate membrane filters with a final pore size of 0.22 μm as shown in Table 1. The surface of the vesicles were modified during spontaneous incorporation of PEG conjugated to 1,2-distearoyl-*sn*-glycero-3-phosphoethanolamine (DSPE) into the lipid bilayer of preformed vesicles. The incorporation efficiency of PEG-DSPE was approximately 85%, independent of the added amount. Theoretically, the surface of PEG (0.3)-[SA-Ve] is not fully covered with PEG chains in mushroom conformation (theoretically calculated covered surface area: 85%), and surface coverage is completed with >0.6 mol% of PEG-DSPE. The ^{99m}Tc-labeling efficiency was approximately 84%, independent of the vesicular formulation. Since the ^{99m}Tc was located in the inner aqueous phase of vesicles encapsulating glutathione, the surface properties would not have been altered by the labeling procedure. The incubation of labeled ^{99m}Tc-vesicles in rabbit serum for 48 h revealed that more than 95% of the incorporated ^{99m}Tc remained in the prepared vesicles, regardless of the composition of the vesicles. Also in human plasma, 98% of incorporated ^{99m}Tc remained with PEG(0.6)-[SA-Ve] at 24 h. These data indicate that the labeling procedure results in a stably labeled vesicle preparation and maintains the ^{99m}Tc within vesicles, even during incubation in plasma at 37 °C.

3.2. Circulation kinetics and biodistribution

First, the circulation kinetics and organ distribution of several formulations were compared to determine the optimized component for targeting bone marrow. For this purpose, scintigraphy was superior to other methods because it was possible to quantitatively determine the organ distribution of the injected vesicles in whole body. The elimination rate of SA-Ve from circulating blood was much faster compared with that of control vesicles (Ve): the circulating half-life times ($t_{1/2}$s) of the SA-Ve and Ve were 0.6 and 9.4 h at injection dose of 15 mg/kg b.w. (Fig. 1(A)). Incorporation of as little as 0.3 mol% of PEG-DSPE did not affect the circulation time of SA-Ve. Incorporation of above 0.6 mol% of PEG-DSPE prolonged the circulation time of SA-Ve and the $t_{1/2}$ increased with increasing amounts of PEG-DSPE incorporation as summarized in Table 1. The incorporation of 2.6 mol% of PEG-DSPE also gave a remarkable improvement in circulation time for control Ve ($t_{1/2}$: 24.8 h). At 24 h post injection, the radioactivity of excised organs was counted using a scintillation counter. Major organs exhibiting the uptake of vesicles were bone marrow and liver for SA-Ve (Figs. 1(B) and (C)), while liver and spleen were the organs with the highest accumulation of control Ve (Figs. 1(C) and (D)). PEG modification clearly inhibited hepatic uptake of both SA-Ve and control Ve, and this effect became significant as the amount of PEG-DSPE incorporated increased (Fig. 1(C)). While a maximum amount of SA-Ve was observed in bone marrow when the SA-Ve contained 0.6 mol% PEG-DSPE, further incorporation of PEG-DSPE led to a decrease in the distribution of SA-Ve in bone marrow (Fig. 1(B)). Other organs apart from kidney and muscle for PEG(2.6)-[SA-Ve] exhibited only a small amount of activity (<1%ID, Supplementary Table 1 online). Injection in rabbits of a mixed solution of ^{99m}Tc-HMPAO and glutathione in a similar ratio as would be found within ^{99m}Tc-vesicles served as a control study of the radiolabeling agents without encapsulation within the vesicles. As shown in Fig. 2(A), injection of ^{99m}Tc-HMPAO/glutathione was rapidly eliminated from blood circulation ($t_{1/2}$: 3 min), and gamma camera images indicated that the labeling agents were rapidly excreted in urine through the kidney (Fig. 2(B)). Region of interest analysis showed that 67.1 ± 0.8% of injected radioactivity was detected in bladder within 1 h after injection (Fig. 2(C)). At 6 h, biodistribution data also showed significant radioactivity in the urine (76.91 ± 4.80%ID) and kidney (6.11 ± 0.53%ID), but other organs including bone marrow had only minimal %ID dose uptake as summarized in Table 2. This control study shows that a mixture of ^{99m}Tc-HMPAO and glutathione is rapidly removed from the blood by renal excretion, which is

Table 1
Specification of prepared vesicles

Sample[a]	Mean diameter ± SD (nm)	PEG-DSPE (mol%)	$t_{1/2}$ (h)[b]
SA-Ve	269 ± 11	0	0.6
PEG(0.3)-[SA-Ve]	276 ± 13	0.3	0.6
PEG(0.6)-[SA-Ve]	273 ± 12	0.6	1.0
PEG(1.4)-[SA-Ve]	275 ± 12	1.4	3.9
PEG(2.6)-[SA-Ve]	274 ± 12	2.6	5.4
Ve	262 ± 43	0	9.4
PEG(2.6)-Ve	259 ± 74	2.6	24.8

[a]SA-Ve is based on DPPC/CH/SA (molar ratio, 1:1:0.2), and Ve is DPPC/CH (molar ratio, 1:1) as a control sample. PEG-modified samples were prepared using the spontaneous incorporation of PEG-DSPE into the prepared SA-Ve or Ve.
[b]The $t_{1/2}$ values were calculated from Fig. 1(A) data.

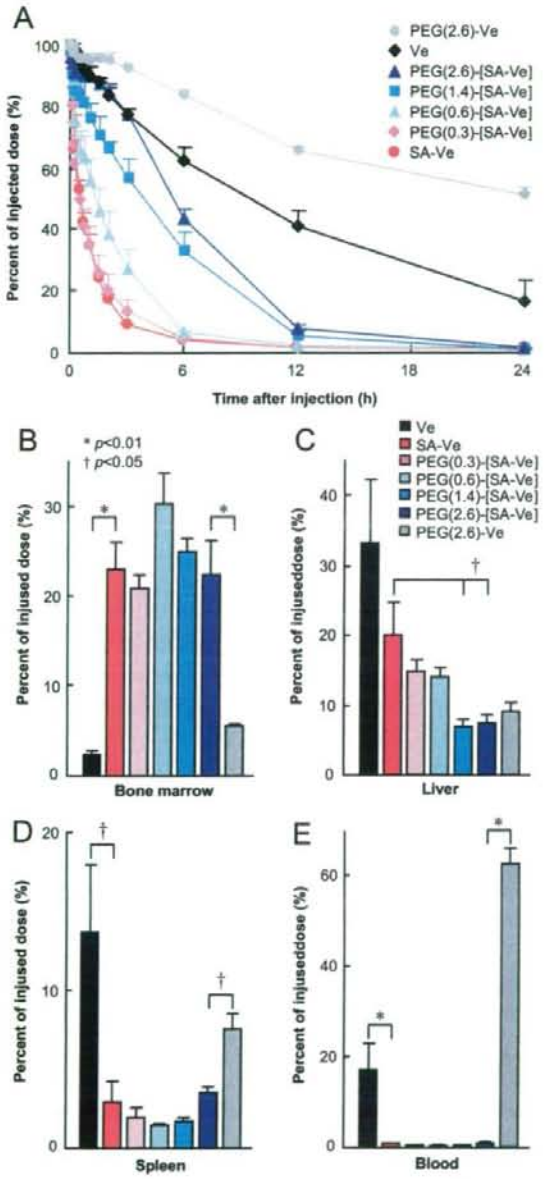

Fig. 1. Effect of surface modification with SA and PEG-DSPE on circulation kinetics and organ distribution of phospholipid vesicles. (A) Circulation kinetics of SA-vesicles (SA-Ve) and control vesicles (Ve) containing various amounts of PEG-DSPE after i.v. infusion (lipids: 15 mg/kg b.w.) in rabbits. ^{99m}Tc radioactivity was quantitated by scintillation counting of blood samples with time. The percentage of injected dose was calculated as a percentage of baseline radioactivity in a blood sample withdrawn just after injection. (B)–(E) Distribution of SA-vesicles (SA-Ve) and control vesicles (Ve) containing various amounts of PEG-DSPE as a percentage of the injected dose in bone marrow (B), liver (C), spleen (D), and blood (E) at 24 h after i.v. infusion in rabbits. *, Statistical significance ($p<0.01$), †, statistical significance ($p<0.05$).

typical of small molecules. These results indicate that the SA-Ve were clearly directed to bone marrow, and the process of accumulation of SA-Ve into bone marrow is correlated with competitive trapping by liver. Surface modification of SA-Ve with the proper amount of PEG-lipids inhibits the trapping of SA-Ve in liver and directs SA-Ve to bone marrow, a process which could be regarded as a combination of active and passive targeting. Conventional anionic vesicles containing phosphatidyl glycerol (PG) were inactive for targeting of bone marrow (Supplementary Table 2 online). The injected PEG(0.6)-[SA-Ve], which was the formulation showing the highest persistence in bone marrow at 24 h, were almost removed from circulation within 6 h (as little as 6.4±0.5%ID of PEG(0.6)-[SA-Ve] was circulating in blood at 6 h). Therefore, the initial distribution kinetics of PEG(0.6)-[SA-Ve] was studied in detail.

3.3. Distribution kinetics of PEG(0.6)-[SA-Ve]

Scintigraphic images clearly showed the injected radioactivity of PEG(0.6)-[SA-Ve] to be redirected from heart and liver, both organs having large blood pool contributions, and increasingly deposited in the bone marrow over time (Fig. 3(A)). The distribution kinetics in bone marrow, liver, and spleen, analyzed from the scintigraphic images, quantitatively indicated that significantly higher doses had accumulated in bone marrow, reaching 68.5±3.3%ID by 6 h after injection (Fig. 3(B)). The biodistribution data calculated from the radioactivity of excised organs also showed that 69.74±0.3%ID of PEG(0.6)-[SA-Ve] had accumulated in bone marrow, as shown in Table 2. At the same time point, liver and spleen had much smaller amounts of 11.51±2.88 and 5.00±1.19%ID, respectively. When ^{99m}Tc-HMPAO/glutathione was injected without encapsulation into PEG(0.6)-[SA-Ve], bone marrow, liver, and spleen had only 1.13±0.24, 1.52±0.14, and 0.01±0.00%ID, respectively. The isolated femur was further separated into soft bone marrow, joint bone (sponge bone), and skeleton and each separate tissue counted for radioactivity. As shown in Fig. 3(C), 66.5±1.1% of radioactivity in one femur was detected in soft bone marrow. The joint bone including soft bone marrow had 28.8±1.3% of radioactivity, and less radioactivity was detected in the separated skeleton (4.7±0.3%). These results indicate that the intravenously injected PEG(0.6)-[SA-Ve] mostly accumulates into soft bone marrow. The gamma camera images clearly show that the bone marrow uptake was evenly distributed over whole bone (Fig. 4), and the localization of radioactivity representing the distribution of PEG(0.6)-[SA-Ve] in these images was analyzed for separate regions. The spine and pelvis had 21.23±0.42% and 18.09±0.60%, values which were much higher than other regions. The right and left femurs had equal radioactivity of 7.97±0.05% and 8.34±0.18%; these values are in agreement with a report

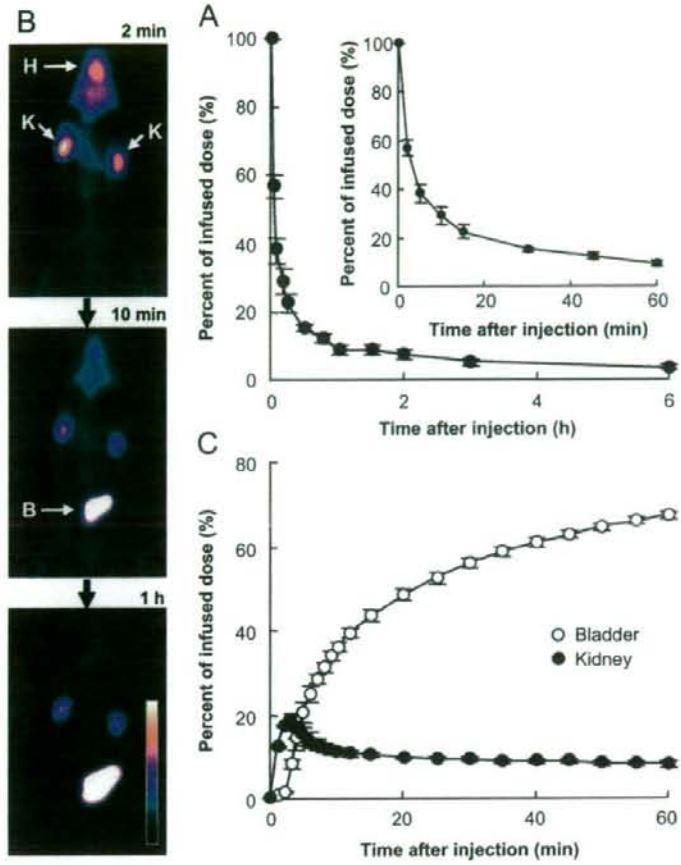

Fig. 2. Circulation and distribution kinetics of mixture of ^{99m}Tc-HMPAO and glutathione without encapsulation in vesicles after i.v. infusion in rabbits. (A) Circulation kinetics (B) Gamma camera images of rabbits acquired at various times after infusion. H: heart, K: kidney, B: bladder. (C) Distribution profiles as a percentage of the injected dose analyzed from the gamma camera images.

describing the relationship of 12 times that of a femur as being equivalent to whole bone in rabbits [28].

3.4. Microscopic localization of PEG(0.6)-[SA-Ve] in bone marrow

The initial studies were designed to demonstrate that PEG(0.6)-[SA-Ve] functions as a nanoparticulate carrier as well as identify their microscopic localization in tissues. We used PEG(0.6)-[SA-Ve] double-labeled by encapsulating water-soluble TR-SOD in an aqueous phase and embedding lipid-soluble C_1-BODIPY C_{12} in bilayer membrane (Fig. 5(A)). As shown in Fig. 5(B), the bone marrow sections have fluorescence from both the TR-SOD and C_1-BODIPY C_{12}. The fluorescence was locally concentrated, and larger fluorescent domain was 30 μm in size along the long axis. Fluorescent distribution in red pulp of spleen was dense, whereas it was sparse in liver. An important finding from this observation is that the fluorescence from membrane probes and encapsulated probes are co-localized in bone marrow. These images clearly indicate that PEG(0.6)-[SA-Ve] functions as a nanoparticle-carrier to deliver the encapsulated agents to bone marrow tissues. A second study was performed to identify the histological location of PEG(0.6)-[SA-Ve] in bone marrow. Femoral bone marrow tissue was taken from rabbit at 6 h after i.v. injection of PEG(0.6)-[SA-Ve] and examined using TEM. TEM observation clearly demonstrated the location of PEG(0.6)-[SA-Ve] in bone marrow (Figs. 6(A) and (B)). A massive number of vesicles were trapped in endosomes and lysosomes of BMMϕ, but no vesicles were observed in cytoplasm and cell nucleus (Fig. 6(B)). The diameter of these vesicles averaged 270 nm which was the original diameter of the intravenously administered PEG(0.6)-[SA-Ve]. Several similar BMMϕ with vesicles in endosomes and lysosomes were observed, while no vesicles were observed

Table 2
Biodistribution of PEG(0.6)-[SA-Ve] and ^{99m}Tc-HMPAO/glutathione as a percent of the injected dose (%ID) and %ID per gram of tissue at 6 h after i.v. infusion in rabbits

Organs	PEG(0.6)-[SA-Ve]		^{99m}Tc-HMPAO/glutathione	
	%ID±SEM (%)	%ID/g tissue±SEM (%/g)	%ID±SEM (%)	%ID/g tissue±SEM (%/g)
Blood	6.58±2.91	0.065±0.028	3.34±1.68	0.025±0.013
Bone marrow	69.74±0.86	0.806±0.048	1.13±0.24	0.010±0.001
Liver	11.51±2.88	0.237±0.067	1.52±0.14	0.022±0.001
Spleen	5.00±1.19	5.387±0.807	0.01±0.00	0.011±0.001
Bowel	5.85±0.31	0.014±0.000	4.41±0.19	0.009±0.000
Skin	1.57±0.21	0.009±0.001	2.34±0.30	0.010±0.001
Kidney	2.40±0.10	0.148±0.011	6.11±0.53	0.440±0.066
Muscle	1.86±0.17	0.003±0.000	2.60±0.63	0.002±0.001
Lung	0.19±0.03	0.024±0.006	0.12±0.03	0.010±0.001
Heart	0.03±0.01	0.010±0.002	0.03±0.01	0.006±0.001
Brain	0.01±0.00	0.002±0.000	0.01±0.00	0.001±0.000
Testis	0.03±0.01	0.024±0.005	0.02±0.00	0.008±0.002
Urine	3.57±1.74	—	76.91±4.80	—

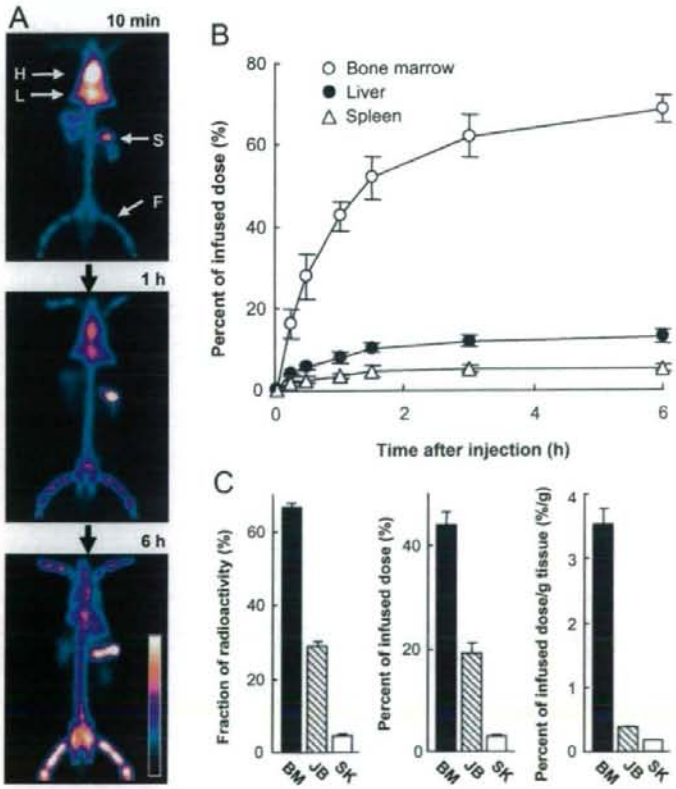

Fig. 3. Initial distribution kinetics of PEG(0.6)-[SA-Ve] after i.v. infusion (lipids: 15 mg/kg b.w.) in rabbits. (A) Gamma camera images of rabbits acquired at various times after infusion. H: heart, L: liver, S: spleen, F: femur. (B) Distribution profiles as a percentage of the injected dose analyzed from the gamma camera images. The total bone marrow was estimated to be 12 times that of one femur. (C) Distribution of radioactivity of PEG(0.6)-[SA-Ve] in separated soft bone marrow (BM), joint bone (sponge bone) (JB), and skeleton (SK) of one femur collected at 6 h after i.v. infusion. Three panels show the fraction of radioactivity, percent of injected dose (%ID), and %ID/g tissue, respectively.

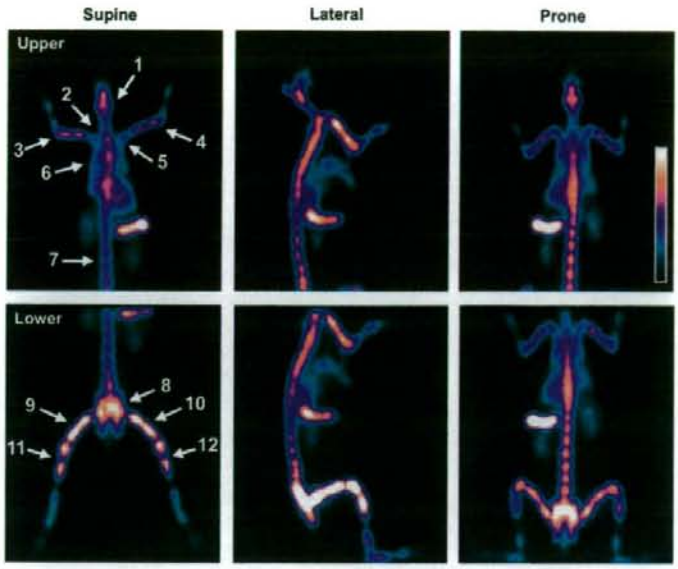

Fig. 4. Gamma camera images of rabbit receiving PEG(0.6)-[SA-Ve], acquired from various angles at 6 h after i.v. infusion. Bone marrow is clearly displayed in these images throughout the rabbit body. Relative radioactivity in separated bone parts were calculated to 1; head (8.41±1.58%), 2; neck (1.10±0.11%), 3; right arm (5.72±0.33%), 4; left arm (5.54±0.40%), 5; shoulder (3.62±0.69%), 6; sternum (4.11±1.35%), 7; spine (21.23±0.42%), 8; pelvis (18.09±0.60%), 9; right femur (7.97±0.05%), 10; left femur (8.34±0.18%), 11; distal right foot (7.88±0.25%), and 12; distal left foot (7.98±0.33%) as percentages to radioactivity of whole bone ± SEM.

in other types of cell such as granular leukocytes, erythroblasts, and endothelial cells in observed section. These microscopic localization studies demonstrate that BMMϕ are the cellular components responsible for clearance of vesicles from the circulation and their uptake by the bone marrow.

4. Discussion

These studies demonstrate that PEG-[SA-Ve] are efficient carriers for targeting the BMMϕ. These vesicles should be useful in the development of bone marrow targeted agents for therapeutic applications. Additionally, this *in vivo* model appears to be an ideal model with which to investigate the role of BMMϕ in the hematopoietic environment. The radiolabeling method for the vesicles encapsulating glutathione with ^{99m}Tc-HMPAO has previously been established for imaging studies [14,23,24]. In the present vesicle formulation, we confirmed the stability of the ^{99m}Tc radiolabeled-vesicles during incubation in serum and plasma at 37 °C for 48 h (more than 95% remaining with vesicles), and we also determined that the free labeling agent is not specifically distributed into organs such as bone marrow, liver, and spleen, but rapidly eliminated through renal excretion as shown in Fig. 2 and Table 2. This evidence provides strong support that the radioisotope distribution reflects the true biodistribution of vesicles. As shown in Fig. 1, comparative data showing the organ distribution of several formulations clearly demonstrated that the uptake of vesicles by bone marrow is induced by the incorporation of SA ($p<0.01$); furthermore, the incorporation of a small amount of PEG-DSPE on the surface of SA-Ve prolongs its circulation time and tends to enhance the bone marrow selectivity by preventing hepatic uptake. Thus, maximum distribution to bone marrow was observed at 0.6 mol% PEG-DSPE (Fig. 1(B)). The degree of hepatic uptake was reduced as the PEG-DSPE content increased, and this effect became significant above 1.4 mol% ($p<0.05$). Bone marrow uptake was also reduced above 1.4 mol%. In general, 5–10 mol% of PEG-lipids is incorporated into most of the long circulating vesicle formulations for passive targeting [8,9]. In the present study, prolonged circulation time of vesicles was observed above 0.6 mol% of PEG-DSPE, and the circulation times were prolonged more in vesicles with higher PEG-DSPE content. For the effective targeting of bone marrow, however, higher concentrations of PEG blocked the active targeting of the vesicles to bone marrow. These results indicate that the dense PEG layer on the vesicular surface covers the surface properties having the character of SA and depress uptake by BMMϕ. Therefore, the optimal amount of PEG incorporation was found to be 0.6 mol%, as this concentration passively enhances active targeting. Theoretically, approximately 0.4 mol% of PEG (Mw 5000)-lipids is estimated to be the critical content required to fully cover the vesicle surface which consists of DPPC and CH (1:1 molar ratio) with the mushroom conformation of PEG chains from Eqs. (1) to (3). Thus, it is

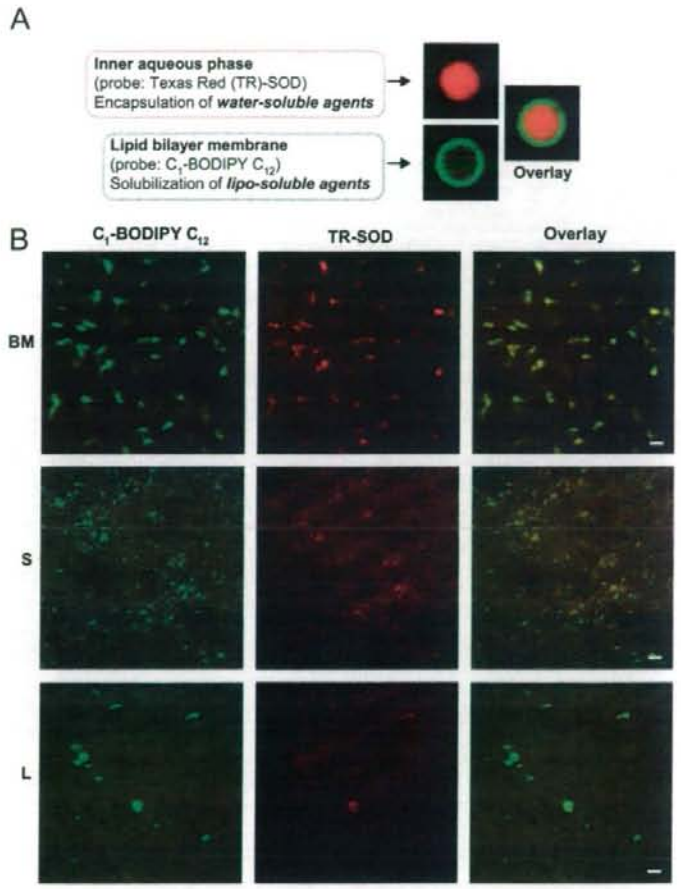

Fig. 5. Histological examination of fluorescence delivered into bone marrow tissues using PEG(0.6)-[SA-Ve] as carriers. (A) Fluorescence localization in double fluorescence-labeled large multilamellar PEG(0.6)-[SA-Ve] with diameter of ca. 10 μm. This observation was performed before extrusion to submicron size to enable observation of the structure within resolution of a confocal microscope. This image indicates that red fluorescence comes from TR-SOD which is encapsulated in inner aqueous phase and green fluorescence comes from C_1-BODIPY C_{12} which is embedded in bilayer membrane. (B) Confocal scanning images of femoral bone marrow (BM), spleen (S), and liver (L) taken from rabbit at 6 h after i.v. injection of double fluorescence-labeled PEG(0.6)-[SA-Ve] with size of 247 ± 22 nm in diameter (lipids: 15 mg/kg b.w.). The scale bars represent 20 μm.

estimated that the optimal incorporation amount of PEG-lipids is slightly higher than that required to fully cover the vesicular surface. This finding provides useful information for the design of vesicle surface to passively enhance the active targeting with PEG-modification *in vivo*.

To examine the participation of the anionic properties of vesicles in BMMϕ uptake, we investigated the organ distribution of conventional anionic vesicles containing PG with same protocol. These PG-vesicles do not distribute to the bone marrow (Supplementary Table 2 online, only 5.36 ± 0.65%ID of PG-vesicles were taken up by the bone marrow at 24 h after i.v. injection). Comparative data for Ve and SA-Ve are shown in Fig. 1(B) and Supplementary Table 1. Previous publications have also supported the observation that PG-vesicles do not distribute to the bone marrow [33], and neutral vesicles with various sizes in the range of 136.2–318 nm do not distribute to the bone marrow [34]. These results indicated that the targeting of bone marrow is not general for neutral vesicles and is achieved not only by the anionic surface of vesicles. The results suggest that SA is specifically responsible for the bone marrow targeting.

Histological observations showed that the vesicles and encapsulated agents are distributed at the same locations into bone marrow tissues, clearly indicating that the encapsulated agents were delivered to the bone marrow tissues by the vesicles (Fig. 5). Higher magnification TEM observations have demonstrated that a massive number of vesicles are trapped in the endosomes and lysosomes of the BMMϕ (Fig. 6). These observations indicated that the

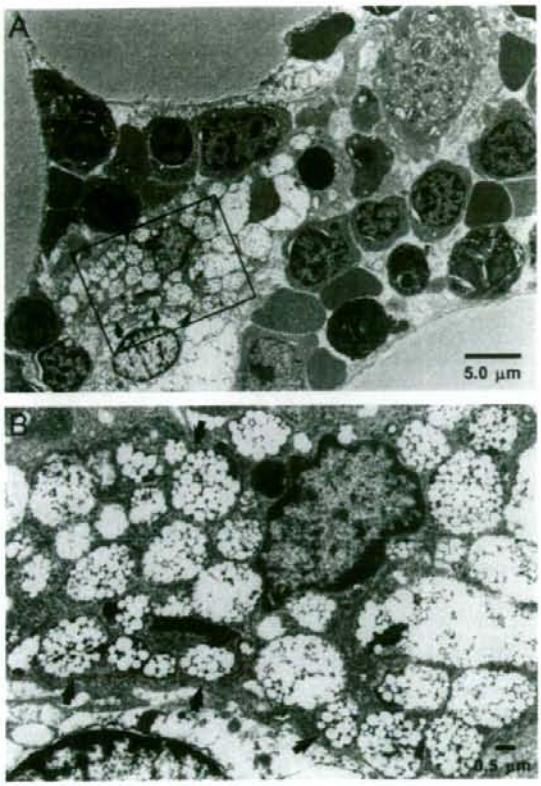

Fig. 6. Transmission electron micrographs of femoral bone marrow tissue section, taken from rabbit at 6 h after i.v. injection of PEG(0.6)-[SA-Ve] (lipids: 15 mg/kg b.w.). (A) Low magnified micrograph representing the bone marrow tissue including macrophage and various bone marrow cells. (B) High magnified micrograph of framed region in panel (A). A massive number of vesicles with original diameter (average 270 nm) are trapped in several endosomes or lysosomes of macrophage. Some are indicated by arrows, which shows same position in (A) and (B).

uptake of PEG(0.6)-[SA-Ve] by bone marrow was responded by the endocytosis of BMMϕ. One potent trigger to accelerate the cellular endocytosis for vesicles is an interaction with the receptors on the surface of cells, that are known as a receptor-mediated endocytosis which is investigated as a potent pathway for drug targeting to specific cell including macrophage [2,10,11]. Scavenger receptors are membrane glycoproteins that are present mainly on cells of the macrophage lineage [35,36]. Various polyanionic compounds such as dextran sulfate, polyinosinic acid, and acetylated low density lipoproteins have been reported as ligands for this receptor [37,38]. These compounds are taken at high levels by macrophages via a scavenger receptor-mediated mechanism. On the other hand, many polyanions such as chondroitin sulfate, poly(D-glutamic) acid, and polycytidylic acid are not ligands for scavenger receptors [37,38]. Previous investigations indicated that the scavenger receptors on macrophages contribute to the recognition of polyanionic structures, resulting in selective uptake. Enhanced uptake of succinylated proteins has been investigated in cultured brain microvessel endothelial cells. Endothelial cells also express the scavenger receptor on their surface. Large succinylated proteins such as catalase (Mw 227 kDa) and bovine serum albumin (Mw 70 kDa) were taken up by the cells via a scavenger receptor-mediated mechanism, whereas significant uptake was not observed for native proteins and small succinylated proteins such as SOD (Mw 34 kDa) and soybean trypsin inhibitor (Mw 21 kDa) [39]. This indicates that succinylation of large molecules is involved in the uptake via a scavenger receptor-mediated mechanism. Recently, Szabó et al. reported the uptake of branched polypeptides by bone marrow culture-derived murine macrophages. They indicated that the succinylation of branched polypeptides significantly enhanced the uptake by macrophages, and the uptake was inhibited by blocking of the class-A scavenger receptors [40]. Because the terminal hydrophilic head group of SA is corresponding to the succinylated structure, we speculate that the interaction between PEG-[SA-Ve] and the scavenger receptors on BMMϕ might participate in the selective uptake. However, further mechanistic investigation on uptake of PEG-[SA-Ve] by BMMϕ, splenic macrophages, and hepatic Kupffer cells is necessary to clarify the mechanism of organ selective macrophage uptake.

Previous pharmacokinetic studies have been performed using vesicles containing SA that have the same lipid composition as in the present study with PEG(0.3)-[SA-Ve], but a significantly higher dose was employed (lipids: 680 mg/kg b.w.) [17]. In these studies, the bone marrow-selective distribution was not observed, so it appears that the bone marrow selectivity is limited by the injection dosage in certain applications. As the vesicle dosage increases, the MPS in the bone marrow becomes saturated; as a result, liver and spleen uptake is increased. In our previous organ distribution study in rabbits, >50%ID of the vesicles were still in circulation at 48 h after infusion of a massive dose of vesicles, while the bone marrow had 7.36 ± 0.34% of 680 mg/kg b.w. at the same time point [17]. This value is equivalent to 50.0 mg/kg b.w., and it can be used to estimate the maximum uptake capacity of MPS for vesicles. When vesicle dosage increases above 50.0 mg/kg b.w., the bone marrow is the first organ to become saturated, and the accumulation of vesicles then increases in the liver and spleen. Such sequential saturation of the MPS eliminates organ selectivity. Therefore, the bone marrow targeting of SA-Ve becomes striking when the dose of vesicles is below the saturation dosage for bone marrow, as observed in the present study (15 mg/kg b.w.). The ability of vesicular nanoparticles to encapsulate a wide variety of agents provides significant opportunities for bone marrow delivery applications. In the present study, we have demonstrated the delivery of scintigraphic and fluorescence imaging agents to bone marrow by using the

SA-Ve vesicles. This method has advantages in delivering the therapeutic agents to treat bone marrow disorders.

5. Conclusion

This is the first report to show the organ distribution of PEG-[SA-Ve] at small dose injection. Organ distributions of several vesicular formulations were quantitatively compared to determine the component to induce the significant distribution into bone marrow. Our data have indicated that surface modification of phospholipid vesicles with two compounds, SA and PEG-DSPE, cooperatively induces the significant bone marrow targeting properties to vesicles. In this system, BMMϕ participated in the uptake of PEG-[SA-Ve], and the efficient delivery of the vesicles as encapsulating agents into the bone marrow was achieved within 6 h after injection. These results indicated that the PEG-[SA-Ve] is a potent carrier for drug delivery into BMMϕ *in vivo* and may be useful for delivering a wide range of therapeutic agents to bone marrow.

Acknowledgments

This work was partly supported by project of a Health and Labor Sciences Research Grant (Research on Pharmaceutical and Medical Safety, Artificial Blood Project) of the Ministry of Health, Labor and Welfare, Japan, and the Ministry of Education, Culture, Sports, Science and Technology, Grant-in-Aid for Scientific Research (B), 17300162, 2005. The authors gratefully acknowledge Dr. H. Sakai (Waseda University) for discussions on this research, Dr. Linda M. McManus (UTHSCSA) for assistance with electron microscopic images and Mr. R. Klipper (UTHSCSA) for technical support.

Appendix A. Supplementary materials

The online version of this article contains additional supplementary data. Please visit doi:10.1016/j.biomaterials.2007.01.041.

References

[1] Farokhzad OD, Jon S, Khademhosseini A, Tran TN, Lavan DA, Langer R. Nanoparticle–aptamer bioconjugates: a new approach for targeting prostate cancer cells. Cancer Res 2004;64:7668–72.
[2] Torchilin VP. Recent advances with liposomes as pharmaceutical carriers. Nat Rev Drug Discov 2005;4:145–60.
[3] Gregoriadis G, Wills EJ, Swain CP, Tavill AS. Drug-carrier potential of liposomes in cancer chemotherapy. Lancet 1974;1:1313–6.
[4] Felgner PL, Gadek TR, Holm M, Roman R, Chan HW, Wenz M, et al. Lipofection: a highly efficient, lipid-mediated DNA-transfection procedure. Proc Natl Acad Sci USA 1987;84:7413–7.
[5] Moghimi SM, Hunter AC, Murray JC. Long-circulating and target-specificity nanoparticles: theory to practice. Pharmacol Rev 2001;53:283–318.
[6] Sakai H, Horinouchi H, Tomiyama K, Ikeda E, Takeoka S, Kobayashi K, et al. Hemoglobin-vesicles as oxygen carriers: influence on phagocytic activity and histopathological changes in reticuloendothelial system. Am J Pathol 2001;159:1079–88.
[7] Fadok VA, Bratton DL, Rose DM, Pearson A, Ezekewitz RA, Henson PM. A receptor for phosphatidylserine-specific clearance of apoptotic cells. Nature 2000;405:85–90.
[8] Klibanov AL, Maruyama K, Torchilin VP, Huang L. Amphipathic polyethyleneglycols effectively prolong the circulation time of liposomes. FEBS Lett 1990;268:235–7.
[9] Gabizon A, Shmeeda H, Barenholz B. Pharmacokinetics of pegylated liposomal Doxorubicin: review of animal and human studies. Clin Pharmacokinet 2003;42:419–36.
[10] Turk MJ, Water DJ, Low PS. Folate-conjugated liposomes preferentially target macrophages associated with ovarian carcinoma macrophage. Cancer Lett 2004;213:165–72.
[11] Chellat F, Merhi Y, Moreau A, Yahia L'H. Therapeutic potential of nanoparticulate systems for macrophage targeting. Biomaterials 2005;26:7260–75.
[12] Mantovani A, Sozzani S, Locati M, Allavena P, Sica A. Macrophage polarization: tumor-associated macrophages as a paradigm for polarized M2 mononuclear phagocytes. Trends Immunol 2002;23:549–55.
[13] Allen TM, Austin GA, Chonn A, Lin L, Lee KC. Uptake of liposomes by cultured mouse bone marrow macrophages: influence of liposome composition and size. Biochim Biophys Acta 1991;1061:56–64.
[14] Phillips WT, Klipper RW, Awasthi VD, Rudolph AS, Cliff R, Kwasiborski V, et al. Polyethylene glycol-modified liposome-encapsulated hemoglobin: a long circulating red cell substitute. J Pharmacol Exp Ther 1999;288:665–70.
[15] Dams ET, Oyen WJ, Boerman OC, Storm G, Laverman P, Kok PJ, et al. ^{99m}Tc-PEG liposomes for the scintigraphic detection of infection and inflammation: clinical evaluation. J Nucl Med 2000;41:622–30.
[16] Giuliani AL, Wiener E, Lee MJ, Brown IN, Berti G, Wickramasinghe SN. Changes in murine bone marrow macrophages and erythroid burst-forming cells following the intravenous injection of liposome-encapsulated dichloromethylene diphosphonate (Cl_2MDP). Eur J Haematol 2001;66:221–9.
[17] Sou K, Klipper R, Goins B, Tsuchida E, Phillips WT. Circulation kinetics and organ distribution of Hb-vesicles developed as a red blood cell substitute. J Pharmacol Exp Ther 2005;312:702–9.
[18] Sadahira Y, Mori M. Role of the macrophage in erythropoiesis. Pathol Int 1999;49:841–8.
[19] Yoshida H, Kawane K, Koike M, Mori Y, Uchiyama Y, Nagata S. Phosphatidylserine-dependent engulfment by macrophages of nuclei from erythroid precursor cells. Nature 2005;437:754–8.
[20] Sou K, Naito Y, Endo T, Takeoka S, Tsuchida E. Effective encapsulation of proteins into size-controlled phospholipid vesicles using freeze–thawing and extrusion. Biotechnol Prog 2003;19:1547–52.
[21] Sou K, Endo T, Takeoka S, Tsuchida E. Poly(ethylene glycol)-modification of the phospholipid vesicles by using the spontaneous incorporation of poly(ethylene glycol)-lipid into the vesicles. Bioconjug Chem 2000;11:372–9.
[22] Sakai H, Hisamoto S, Fukutomi I, Sou K, Takeoka S, Tsuchida E. Detection of lipopolysaccharide in hemoglobin-vesicles by Limulus amebocyte lysate test with kinetic-turbidimetric gel clotting analysis and pretreatment of surfactant. J Pharm Sci 2004;93:310–21.
[23] Rudolph AS, Klipper R, Goins B, Phillips WT. *In vivo* biodistribution of a radiolabeled blood substitute: ^{99m}Tc-labeled liposome-encapsulated hemoglobin in an anesthetized rabbit. Proc Natl Acad Sci USA 1991;88:10976–80.
[24] Phillips WT, Rudolph AS, Goins B, Timmons JH, Klipper R, Blumhardt R. A simple method for producing a technetium-99m-labeled liposome which is stable *in vivo*. Nucl Med Biol 1992;19:539–47.

[25] Awasthi V, Goins B, Klipper R, Loredo R, Korvick D, Phillips WT. Dual radiolabeled liposomes: biodistribution studies and localization of focal sites of infection in rats. Nucl Med Biol 1998;25:155–60.
[26] Kozma C, Macklin W, Cummins LM, Mauer R. Anatomy, physiology, and biochemistry of the rabbit. In: Weisbroth SH, Flatt RE, Kraus AL, editors. The biology of the laboratory rabbit. New York: Academic Press; 1974. p. 50–69.
[27] Kaplan HM, Timmons EH. The rabbit: a model for the principles of mammalian physiology and surgery. New York: Academic Press; 1979.
[28] Deitz AA. Distribution of bone marrow, bone and bone ash in rabbits. Proc Soc Exp Med 1944;57:60–2.
[29] Lefevre C, Kang HC, Haugland RP, Malekzadeh N, Arttamangkul S, Haugland RP. Texas Red-X and rhodamine Red-X, new derivatives of sulforhodamine 101 and lissamine rhodamine B with improved labeling and fluorescence properties. Bioconjug Chem 1996;7:482–9.
[30] Torchilin VP, Papisov MI. Why do polyethylene glycol-coated liposomes circulate so long? J Liposome Res 1994;4:725–39.
[31] Du H, Chandaroy P, Hui SW. Grafted poly-(ethylene glycol) on lipid surface inhibits protein adsorption and cell adhesion. Biochim Biophys Acta 1997;1326:236–48.
[32] Edholm O, Nagle JF. Areas of molecules in membranes consisting mixtures. Biophys J 2005;89:1827–32.
[33] Awasthi VD, Garcia D, Klipper R, Goins BA, Phillips WT. Neutral and anionic liposome-encapsulated hemoglobin: effect of postinserted poly(ethylene glycol)-distearoylphosphatidylethanolamine on distribution and circulation kinetics. J Pharmacol Exp Ther 2004; 309:241–8.
[34] Awasthi VD, Garcia D, Goins BA, Phillips WT. Circulation and biodistribution profiles of long-circulating PEG-liposomes of various sizes in rabbits. Int J Pharm 2003;253:121–32.
[35] Doi T, Higashino K, Kurihara Y, Wada Y, Miyazaki T, Nakamura H, et al. Charged collagen structure mediates the recognition of negatively charged macromolecules by macrophage scavenger receptors. J Biol Chem 1993;268:2126–33.
[36] Taylor PR, Martinez-Pomares L, Stacey M, Lin HH, Brown GD, Gordon S. Macrophage receptors and immune recognition. Annu Rev Immunol 2005;23:901–44.
[37] Brown MS, Goldstein JL. Lipoprotein metabolism in the macrophage: implications for cholesterol deposition in atherosclerosis. Annu Rev Biochem 1983;52:223–61.
[38] Krieger M, Acton S, Ashkenas J, Pearson A, Penman M, Resnick D. Molecular flypaper, host defense, and atherosclerosis. Structure, binding properties, and functions of macrophage scavenger receptors. J Biol Chem 1993;268:4569–72.
[39] Tokuda H, Masuda S, Takakura Y, Sezaki H, Hashida M. Specific uptake of succinylated proteins via a scavenger receptor-mediated mechanism in cultured brain microvessel endothelial cells. Biochem Biophys Res Commun 1993;196:18–24.
[40] Szabó R, Peiser L, Plüddemann A, Bösze S, Heinsbroek S, Gordon S, et al. Uptake of branched polypeptides with poly[L-lys] backbone by bone-marrow culture-derived murine macrophages: the role of the class a scavenger receptor. Bioconjug Chem 2005;16:1442–50.

Rheological Properties of Hemoglobin Vesicles (Artificial Oxygen Carriers) Suspended in a Series of Plasma-Substitute Solutions

Hiromi Sakai,[†] Atsushi Sato,[‡] Shinji Takeoka,[‡] and Eishun Tsuchida*[,†]

Advanced Research Institute for Science and Engineering and Graduate School of Science and Engineering, Waseda University, Tokyo 169-8555, Japan

Received February 15, 2007. In Final Form: April 3, 2007

Hemoglobin vesicles (HbV) or liposome-encapsulated Hbs are artificial oxygen carriers that have been developed for use as transfusion alternatives. The extremely high concentration of the HbV suspension (solutes, ca. 16 g/dL; volume fraction, ca. 40 vol %) gives it an oxygen-carrying capacity that is comparable to that of blood. The HbV suspension does not possess a colloid osmotic pressure. Therefore, HbV must be suspended in or co-injected with an aqueous solution of a plasma substitute (water-soluble polymer), which might interact with HbV. This article describes our study of the rheological properties of HbV suspended in a series of plasma substitute solutions of various molecular weights: recombinant human serum albumin (rHSA), dextran (DEX), modified fluid gelatin (MFG), and hydroxylethyl starch (HES). The HbV suspended in rHSA was nearly Newtonian. Other polymers—HES, DEX, and MFG—induced HbV flocculation, possibly by depletion interaction, and rendered the suspensions as non-Newtonian with a shear-thinning profile (10^{-1}−10^{3} s^{-1}). These HbV suspensions showed a high storage modulus (G') because of the presence of flocculated HbV. However, HbV suspended in rHSA exhibited a very low G'. The viscosities of HbV suspended in DEX, MFG, and high-molecular-weight HES solutions responded quickly to rapid step changes in shear rates of 0.1−100 s^{-1} and a return to 0.1 s^{-1}, indicating that flocculation is both rapid and reversible. Microscopically, the flow pattern of the flocculated HbV that perfused through microchannels (4.5 μm deep, 7 μm wide, 20 cmH_2O applied pressure) showed no plugging. Furthermore, the time required for passage was simply proportional to the viscosity. Collectively, the HbV suspension viscosity was influenced by the presence of plasma substitutes. The HbV suspension provides a unique opportunity to manipulate rheological properties for various clinical applications in addition to its use as a transfusion alternative.

Introduction

Phospholipid vesicles or liposomes encapsulating or embedding functional drugs or biological materials have been investigated aggressively for use in drug-delivery systems; some were subsequently approved for antifungal or anticancer therapy.[1] Hemoglobin vesicles (HbV) are artificial oxygen carriers that encapsulate a concentrated Hb solution in phospholipid vesicles (280 nm particle diameter).[2−6] Their oxygen-carrying capacity and safety as a transfusion alternative have been evaluated energetically in animal tests aimed at clinical applications. In contrast to conventional liposomal products, the concentration of the HbV suspension must be extremely high (Hb, 10 g/dL; lipids, 5−6 g/dL); one injection as a transfusion alternative causes the substitution of a large volume of blood: about 40% of the circulating blood volume.[7] Accordingly, it is important to evaluate its safety not only in terms of the biocompatibility of the HbV particles themselves but also in terms of the rheological property of the HbV suspension, the infusion fluid, compared to the blood hemorheology.[8−10]

Albumin, dissolved in a blood plasma at ca. 5 g/dL, provides sufficient colloid osmotic pressure (COP, ca. 20 Torr) to play an important role in equilibrating COP between blood and interstitial fluid, thereby maintaining the overall blood volume. This COP is one requisite for a transfusion alternative to sustain blood circulation for transporting oxygen and metabolites. One HbV contains about 30 000 Hb molecules. Therefore, an HbV suspension shows no COP in an aqueous solution. Accordingly, HbV must be suspended in or co-injected with a plasma substitute solution. This requirement is identical to that for emulsified perfluorocarbon, which does not possess COP;[11,12] it contrasts with characteristics of other Hb-based oxygen carriers (HBOCs), intramolecular cross-linked Hbs, polymerized Hbs, and polymer-conjugated Hbs, which all possess very high COP as protein solutions.[13−15]

Animal tests of HbV suspended in plasma-derived human serum albumin (HSA) or recombinant HSA (rHSA) showed an oxygen-transporting capacity that is comparable to that of

* To whom correspondence should be addressed. E-mail: eishun@waseda.jp. Tel: +81-3-5286-3120. Fax: +81-3-3205-4740.

† Advanced Research Institute for Science and Engineering.

‡ Graduate School of Science and Engineering.

(1) Torchilin, V. P. *Nat. Rev. Drug Discovery* **2005**, *4*, 145−160.

(2) Izumi, Y.; Sakai, H.; Hamada, K.; Takeoka, S.; Yamahata, T.; Kato, R.; Nishide, H.; Tsuchida, E.; Kobayashi, K. *Crit. Care Med.* **1996**, *24*, 1869−1873.

(3) Sakai, H.; Takeoka, S.; Park, S. I.; Kose, T.; Nishide, H.; Izumi, Y.; Yoshizu, A.; Kobayashi, K.; Tsuchida, E. *Bioconjugate Chem.* **1997**, *8*, 23−30.

(4) Chang, T. M. *Artif. Organs* **2004**, *28*, 789−794.

(5) Djordjevich, L.; Miller, I. F. *Exp. Hematol.* **1980**, *8*, 584−592.

(6) Phillips, W. T.; Klipper, R. W.; Awasthi, V. D.; Rudolph, A. S.; Cliff, R.; Kwasiborski, V.; Goins, B. A. *J. Pharmacol. Exp. Ther.* **1999**, *288*, 665−670.

(7) Sakai, H.; Horinouchi, H.; Yamamoto, M.; Ikeda, E.; Takeoka, S.; Takaori, M.; Tsuchida, E.; Kobayashi, K. *Transfusion* **2006**, *46*, 339−347.

(8) Makino, C.; Kimura, N.; Hasegawa, E.; Tsuchdia, E. *Nippon Kagaku Kaishi* **1991**, *8*, 1102−1105.

(9) Sakai, H.; Hamada, K.; Takeoka, S.; Nishide, H.; Tsuchida, E. *Biotechnol. Prog.* **1996**, *12*, 119−125.

(10) Chung, T. W.; Huang, Y. Y.; Wu, C. I. *Artif. Cells. Blood Substitutes. Immobilization Biotechnol.* **1999**, *27*, 215−227.

(11) Nolte, D.; Pickelmann, S.; Lang, M.; Keipert, P.; Messmer, K. *Anesthesiology* **2000**, *93*, 1261−1270.

(12) Jouan-Hureaux, V.; Audonnet-Blaise, S.; Lacatusu, D.; Krafft, M. P.; Dewachter, P.; Cauchois, G.; Stoltz, J. F.; Longrois, D.; Menu, P. *Transfusion* **2006**, *46*, 1892−1898.

(13) Sakai, H.; Yuasa, M.; Onuma, H.; Takeoka, S.; Tsuchida, E. *Bioconjugate. Chem.* **2000**, *11*, 56−64.

(14) Vandegriff, K. D.; McCarthy, M.; Rohlfs, R. J.; Winslow, R. M. *Biophys. Chem.* **1997**, *69*, 23−30.

(15) Manjula, B. N.; Tsai, A.; Upadhya, R.; Perumalsamy, K.; Smith, P. K.; Malavalli, A.; Vandegriff, K.; Winslow, R. M.; Intaglietta, M.; Prabhakaran, M.; Friedman, M. J.; Acharya, A. S. *Bioconjugate Chem.* **2003**, *14*, 464−472.

10.1021/la7004503 CCC: $37.00
Published on Web 06/13/2007